HHS Public Access

Author manuscript

Oncogene. Author manuscript; available in PMC 2020 June 05.

Published in final edited form as:

Oncogene. 2020 March ; 39(10): 2103–2117. doi:10.1038/s41388-019-1136-4.

The Mechanism of Cancer Drug Addiction in ALK-Positive T-Cell Lymphoma

Soumya S. Rajan[1,2], **Amit Dipak Amin**[2,3], **Lingxiao Li**[2,3], **Delphine C. Rolland**[4], **Haiquan Li**[5], **Deukwoo Kwon**[2,6], **Mercedes F. Kweh**[2,3], **Artavazd Arumov**[1,2], **Evan R. Roberts**[2], **Aimin Yan**[2], **Venkatesha Basrur**[7], **Kojo S.J Elenitoba-Johnson**[4], **Xi Steven Chen**[2,6], **Soham D. Puvvada**[8], **Yves A. Lussier**[8,9], **Daniel Bilbao**[2], **Megan S. Lim**[4], **Jonathan H. Schatz**[2,3]

[1]Sheila and David Fuente Graduate Program in Cancer Biology, University of Miami Miller School of Medicine, Miami, FL

[2]Sylvester Comprehensive Cancer Center, University of Miami Miller School of Medicine, Miami, FL

[3]Division of Hematology, Department of Medicine, University of Miami Miller School of Medicine, Miami, FL

[4]Department of Pathology and Laboratory Medicine, Perelman School of Medicine, University of Pennsylvania, Philadelphia, PA

[5]Department of Biosystems Engineering, University of Arizona, Tucson, AZ

[6]Department of Public Health Sciences, University of Miami Miller School of Medicine, Miami, FL

[7]Department of Pathology, University of Michigan, Ann Arbor, MI

[8]Department of Medicine, Bio5 Institute, UA Cancer Center, Tucson, AZ

[9]Interdisciplinary Program in Statistics, University of Arizona, Tucson, AZ

Abstract

Rational new strategies are needed to treat tumors resistant to kinase inhibitors. Mechanistic studies of resistance provide fertile ground for development of new approaches. Cancer drug addiction is a paradoxical resistance phenomenon, well-described in MEK-ERK-driven solid tumors, in which drug-target overexpression promotes resistance but a toxic overdose of signaling if inhibitor is withdrawn. This can permit prolonged control of tumors through intermittent dosing. We and others showed previously that cancer drug addiction arises also in the hematologic malignancy ALK-positive anaplastic large-cell lymphoma (ALCL) resistant to ALK-specific tyrosine kinase inhibitors (TKIs). This is driven by overexpression of the fusion kinase NPM1-ALK, but the mechanism by which ALK overactivity drives toxicity upon TKI withdrawal

Corresponding Author: Jonathan Schatz, 1580 NW 10th Avenue, Batchelor Children Research Building, Rm 415, University of Miami Miller School of Medicine, Miami, FL, 33137; jschatz@med.maimi.edu, Phone: +1-3052434785.

CONFLICT OF INTEREST

The authors declare no conflict of interest.

Supplementary information is available at *Oncogene*'s website

remained obscure. Here we reveal the mechanism of ALK-TKI addiction in ALCL. We interrogated the well-described mechanism of MEK/ERK pathway inhibitor addiction in solid tumors and found it does not apply to ALCL. Instead, phosphoproteomics and confirmatory functional studies revealed STAT1 overactivation is the key mechanism of ALK-TKI addiction in ALCL. Withdrawal of TKI from addicted tumors in vitro and in vivo leads to overwhelming phospho-STAT1 activation, turning on its tumor-suppressive gene-expression program and turning off STAT3's oncogenic program. Moreover, a novel NPM1-ALK-positive ALCL PDX model showed significant survival benefit from intermittent compared to continuous TKI dosing. In sum, we reveal for the first time the mechanism of cancer-drug addiction in ALK-positive ALCL and the benefit of scheduled intermittent dosing in high-risk patient-derived tumors in vivo.

Introduction

Targeted kinase inhibitors provide active treatments for many cancers but uncommonly promote durable responses due to de novo and acquired resistance.[1] Refractory disease driven by overexpression or mutations of the targeted kinase or activation of alternate signaling pathways inevitably emerge in most clinical scenarios, and affected patients require new strategies. Cancer drug addiction is a paradoxical resistance phenomenon that can prolong control of some solid tumors in vivo through intermittent dosing.[2–4] Specifically, melanomas and lung cancers with MEK/ERK activation downstream of BRAF or EGFR activation may develop resistance due to overexpression of pathway intermediates, but this promotes toxic hyperactivation of signaling when inhibitor is not present. In BRAF-V600E-driven melanomas, prolonged control of patient-derived xenograft tumors in mice through intermittent dosing prompted an ongoing clinical trial (NCT02583516).[5] Mechanisms driving addiction, however, remained obscure until recently when elegant work by the Peeper group showed that in both melanomas and lung cancers, signaling overdose is driven by an ERK2-dependent phenotype switch mediated by the transcription factors JUNB and FRA1.[6]

We previously reported the first major example of cancer-drug addiction in a hematologic malignancy, ALK-positive anaplastic large cell lymphoma (ALCL).[7] ALCL is a T-cell non-Hodgkin lymphoma affecting adults and children. Approximately 70% of cases are driven by the anaplastic lymphoma kinase (ALK) due to reciprocal chromosomal translocations creating a fusion kinase, most commonly *NPM1-ALK* due to t(2;5) (p23:q25).[8] ALK-specific clinical tyrosine kinase inhibitors (TKIs), developed for use in ALK-positive lung cancer,[9,10] show strong activity as salvage therapy for patients with relapsed or refractory ALCL,[11,12] but resistance mechanisms are poorly understood. We showed preclinically that over-expression of *NPM1-ALK* emerges in ALCL cells resistant to ALK inhibitors but drives a toxic over-activation of signaling when inhibitor is withdrawn.[7] Other investigators have validated and elaborated on this cancer drug addiction phenotype in ALK-positive ALCL.[13,14] The mechanism driving toxicity via NPM1-ALK kinase overactivity, however, remained unclear.

Important questions therefore remain regarding the NPM1-ALK kinase, which both drives ALK-positive ALCL and may be found also in ALK-positive diffuse large B-cell lymphoma

(DLBCL).[15,16] Here we sought to understand how this potently oncogenic fusion kinase can become a toxic liability to cells at higher expression levels, the degree of overlap if any with the mechanism described for MEK/ERK overactivation in solid tumors, and whether mechanisms can inform novel treatments. MEK/ERK activation is one of three main signaling consequences of ALK kinase domain-containing fusion oncoproteins, along with AKT/mTOR and JAK/STAT3.[17,18] The possibility therefore that MEK/ERK drives the toxicity of ALK signaling overdose in a manner similar to BRAF and EGFR is logical and was suggested by others.[13] We report here, however, that inhibition of MEK/ERK activation downstream from ALK consistently fails to rescue cells from the effects of ALK overdose. We used phosphoproteomics to identify direct phospho-targets of NPM1-ALK uniquely associated with ALK-driven death. Of these, the tumor suppressive transcription factor STAT1 emerged as key driver of toxicity, working by activating its tumor-suppressive gene-expression program and counteracting the STAT3 program upon which ALCL cells normally depend for survival.[19] Importantly, a novel PDX model of ALK-positive ALCL demonstrates prolonged control of tumors in vivo employing a simple two-week on/off intermittent-dosing strategy.

Results

Co-selection for resistance and addiction in ALCL by all generations of ALK TKI

All ALK-kinase inhibitors approved or under development show high potency against NPM1-ALK-driven ALCL cells (Supplementary Figure 1a). To build on our previous findings that crizotinib and ceritinib generate resistance in ALCL through over-expression of *NPM1-ALK*, we carried out resistance selections using additional inhibitors including alectinib and the potent third-generation inhibitor lorlatinib.[20,21] Selections consistently led to resistance and addiction in parallel. Karpas-299 and SU-DHL-1 cells selected for ability to grow in 100 nM lorlatinib show bell-shaped viability in response to all ALK inhibitors (Figure 1a). These curves are a classic indication of cancer drug-addiction, showing both viability stimulation up to an optimal concentration and ongoing dependence on the drug target, indicated by the viability decline above the optimal concentration.[2,7] Results were similar for selections in alectinib to 150 nM (Supplementary Figure 1b). Confirming TKI addiction, resistant subclones proliferate well in inhibitor but fail to do so in their absence, the reverse phenotype of parental cells (Figure 1b). Microscopic evaluation of drug-addicted cells undergoing cell death after withdrawal of TKI show cell shrinkage followed by blebbing and separation of cell fragments into apoptotic bodies by day 4 (Figure 1c, complete time course including zoomed-in images shown in Supplementary Figure 1c), consistent with our previous findings that ALK TKI-addicted cells undergo apoptosis after drug withdrawal.[7] Resistant clones show increased expression of *NPM1-ALK* mRNA and protein compared to their respective parent (Figure 1d–e). All generations of ALK TKI therefore drive ALK-positive ALCL cells to develop resistance due to NPM1-ALK over expression, leading to the drug-addiction phenotype.

ALK's canonical downstream pathways do not mediate TKI addiction in NPM1-ALK over-expressing resistant ALCL cells

MEK/ERK overactivation drives cancer drug addiction in resistant BRAF-mutant melanomas and MAPK-driven NSCLC, mediated by ERK2 activation of a tumor suppressive gene-expression program.[6] We therefore assessed this pathway as the initial candidate driver of ALK-TKI addiction in ALK-positive ALCL. We tested drugs targeting MEK/ERK signaling molecules in the cell line K299-CR1000, derived from the ALK-positive ALCL line Karpas-299 and selected for ability to tolerate crizotinib in vitro up to 1 000 nM.[7] This well-characterized line requires continuous presence of ALK TKI at optimal concentration to avoid apoptosis, with both resistance and addiction stemming from *NPM1-ALK* overexpression driven by genomic amplification. K299-CR1000 cells washed out of TKI show bell-shaped viability stimulation in response to ALK TKIs but no hint of viability stimulation by drugs targeting MEK1/2, ERK1/2 or the ERK2-selective inhibitor ulixeritinib (Figure 2a). Because of dynamic rewiring of TKI signaling that may arise during MEK inhibition,[22] we confirmed lack of rescue by both MEK inhibitors at multiple time points (Supplementary Figure 2a). We also assessed proliferation, showing as expected growth of K299-CR1000 cells in ALK TKI and loss of all live cells from culture upon plating in vehicle (Figure 2b). MEK/ERK inhibitors promoted no rescue of proliferation, similar to vehicle. We confirmed the concentrations of MEK inhibitors used resulted in inhibition of downstream ERK1/2 phosphorylation, despite the lack of rescue from ALK-TKI withdrawal (Supplementary Figure 2b). Interrogation by MEK/ERK inhibitors therefore revealed no evidence of rescue from NPM1-ALK over-activation in a well-characterized system of ALK TKI addiction.

We therefore sought a more comprehensive picture by interrogating additional targets downstream from NPM1-ALK and employing additional systems of ALK TKI addiction. We screened a large number of inhibitors for ability to rescue from ALK overdose in K299-CR1000 cells plus additional resistant ALK-positive ALCL clones with the TKI-addiction phenotype. These previously characterized lines are derived from Karpas-299, SU-DHL-1, or SUP-M2 ALK-positive ALCL lines and selected for growth in crizotinib (denoted CR) or ceritinib (LDK378, denoted LR).[7] For consistency of analysis, we developed concentration-weighted area under the curve (wAUC) to assess inhibitors' ability to rescue cell viability after TKI washout (Figure 2c). The method quantifies drug effects on viability so results from multiple inhibitors and replicates can be compared across experiments and cell lines. A hypothetical inhibitor with no effect positive or negative on viability (Figure 2c, inhibitor 2) would have wAUC = 1, while those inhibiting viability (inhibitor 1) have wAUC <1. Those that stimulate viability (inhibitors 3 and 4) have wAUC > 1, with the value weighted to reflect higher potency (peak stimulation at lower drug concentration). Mean wAUC values for K299-CR1000 (Figure 2d) were calculated from raw curves (Supplementary Figure 2c, Figure 2a for MEK/ERK inhibitors) after washout from ALK TKI then plating in serial dilutions of the indicated inhibitors. In addition to MEK/ERK, we assessed JAK/STAT3 and PI3K/AKT/mTOR signaling and a variety of additional NPM1-ALK targets: PKM2 (TEPP-46),[23] phospholipase C (U73122),[24] JNK (JNK-IN-8),[25,26] PKC (Ro-31-822),[25] and GSK3ß (GSK-3B-IX).[27] All ALK inhibitors rescued viability of the TKI-addicted cells, with more potent later-generation compounds generally doing so at lower concentration, but

inhibitors of none of the other targets did. Although the JAK inhibitor AZD1480 did increase viability, this compound has known off-target activity against ALK itself.[28] Since no other JAK/STAT inhibitor produced any effect, we conclude the effect of this drug was due to off-target ALK inhibition. Results for additional TKI-addicted resistant lines were similar (Figure 2e, Supplementary Figure 2d, not all drugs were tested in all lines). Comprehensive assessment of NPM1-ALK downstream oncogenic targets using a targeted-inhibitor approach therefore revealed none as a mediator of TKI addiction.

For further confirmation that ALK's three main downstream oncogenic pathways do not mediate TKI addiction, we infected parental ALK-positive ALCL cells with alleles activating them, specifically constitutively active *STAT3C,*[29] an shRNA targeting *PTEN*, and constitutively active *MEK1*-S218D, S222D.[30] As expected, additional *NPM1-ALK* was strongly disadvantageous, consistent with induction of ALK overdose signaling like inhibitor withdrawal from drug-addicted cells (Figure 2f). *STAT3C*, sh*PTEN*, and *MEK1*-S218D, S222D, by contrast, behaved like empty vector or kinase-dead (KD) NPM1-ALK, resulting in no growth disadvantage compared to uninfected cells. Western blotting confirmed expression and activity of pathway-activating alleles (Supplementary Figure 2e). In sum, we find NPM1-ALK over-activity does not drive impaired cell fitness through any of its well established downstream oncogenic signaling pathways, but the effect is clearly ALK-kinase dependent, shown by the strong, consistent rescue by all ALK TKIs. We hypothesized NPM1-ALK over-activation toxicity is driven by a direct ALK-kinase substrate not normally associated with malignant transformation.

Phosphoproteomics yields candidate drivers of NPM1-ALK overdose toxicity

We therefore sought unbiased identification of phosphorylated substrates associated with ALK-overdose. We employed mass-spectrometry proteome-wide assessment of phosphorylation to interrogate phospho-proteins in the K299-CR1000 line upon NPM1-ALK overdose at 12 hours post drug withdrawal, compared to parental cells, with log2 fold enrichment ≥1.5 considered significant (Figure 3a).[23,31] To focus results on phospho-targets associated specifically with NPM1-ALK overactivity, we compared parental Karpas-299 cells growing without drug (Figure 3b, ALK-on, viable) to drug-addicted K299-CR1000 cells following TKI washout (ALK-on, death) revealing a total of 1,871 upregulated phosphoproteins of which 1,750 were in both (common ALK targets, Supplementary Table 1). We then compared K299-CR1000 undergoing overdose (ALK-on, death) to parental cells exposed to ALK TKI (ALK-off, death) and found a total of 213 deregulated targets of which 176 were common to both (common death targets, Supplementary Table 2). This left 21 uniquely deregulated, significantly enriched phospho-targets in the ALK-overdosing cells, which we considered candidate drivers of toxicity (Figure 3c). Gene ontology (GO) annotation showed most are in core bioenergetic and synthetic pathways, which could simply be a consequence of hyper-stimulation by multiple growth and survival pathways downstream of hyper-activated ALK kinase. Since Figure 2 suggested death is mediated by a direct NPM1-ALK substrate instead of its downstream pathways, we identified those candidates whose increased phosphorylation occurs on a tyrosine residue in a consensus ALK (YXXYXXY) phosphorylation motif. [32] Eight proteins showed elevated phosphorylation in such a motif: RSSA, CBLB, CCD50, NYAP2, PEAK1, MET, BCAP, and

STAT1 (Figure 3d, Supplementary Figure 3). As indicated, some of these residues are associated with previously described regulatory functions of these targets.[33–38] Phosphoproteomics therefore revealed candidate NPM1-ALK substrates uniquely associated with overdose toxicity. These data also suggest deregulation of biosynthetic, metabolic, and catabolic processes occurs as a central derangement in cells experiencing NPM1-ALK over-stimulation.

STAT1 activation drives NPM1-ALK overdose-mediated cell death

Identification of STAT1-Y701 phosphorylation as a candidate driver was intriguing because this residue is a known substrate of cytoplasmic NPM1-ALK in ALCL.[38] This normally leads to proteasomal degradation of STAT1 to prevent antagonism of the STAT3 transcriptional program that is the core survival pathway of ALCL.[19] Y701 phosphorylation in other contexts, however, indicates STAT1 activation.[39,40] We therefore interrogated the status of STAT1 and its phosphorylation at Y701 in cells undergoing NPM1-ALK overdose, revealing massive up-regulation of STAT1 phosphorylation (pSTAT1) following ALK TKI washout from drug-addicted lines (Figure 4a). Corresponding increase in the apoptotic transcription factor IRF1, product of a key pSTAT1 target gene,[41–43] suggested strong activation of the tumor-suppressive pSTAT1 gene-expression program was occurring. We therefore performed RNA-seq on five ALK TKI-addicted subclones and their parents with and without TKI. RNA from 5 biological replicates of subclones maintained viably in the presence of TKI (100 nM ceritinib) or induced to enter NPM1-ALK overdose for 12 hours through TKI washout. The three parental lines that gave rise to these clones also were analyzed without inhibitor and after 12 hours in 100 nM ceritinib. We analyzed each death state compared to its corresponding viable state and performed n-of-1 pathway analysis as described[44] (complete GO-annotated heat map of gene-level targets, Supplementary Figure 4a, gene names in Supplementary Table 3). As in the phosphoproteomics, we again observed activation of biosynthetic and metabolic pathways associated with ALK-overdose (group I in Supplementary Figure 4a). Analysis specifically of STAT1 and STAT3 target genes[45,46] showed dramatic up-regulation of STAT1 targets in the ALK-overdose death state, while STAT3 targets were even more strongly lost than in parental lines exposed to ALK TKI (Figure 4b). We verified these findings by qPCR for specific targets in independent samples from multiple drug-addicted subclone-parent pairs (Supplementary Figure 4b). Massive activation of tumor-suppressive pSTAT1-mediated gene expression therefore occurs upon withdrawal of TKI from drug-addicted ALK-positive resistant clones.

For further assessment, we infected parental Karpas-299, SUP-M2, and L-82 cells with constitutively active STAT1C (Arg656Cys, Asn658Cys)[47] and assessed GFP co-expression, compared to *NPM1-ALK* and vector. *STAT1C* showed potent negative selection similar to *NPM1-ALK* (Figure 4c). We also assessed whether *STAT1* knockdown would rescue cells from TKI withdrawal in addicted cells. We infected K299-CR1000 and SUP-CR500 cells maintained in ALK TKI with GFP co-expressing shSCR (scrambled) and two different sh*STAT1* constructs that knocked down STAT1 protein. We withdrew the cells from TKI to induce ALK overdose and then rescued them by restoring TKI. Both sh*STAT1* constructs show significant enrichment as the cells are taken through cycles of overdose and rescue, while shSCR was unchanged (Figure 4d). Overall, results predict pSTAT1 induction by

interferon-gamma (IFNγ) might be toxic to ALK-positive ALCL tumors, especially in combination with ALK TKIs. Indeed, IFNγ has a significant detrimental effect on the viability of ALK-positive ALCL tumors and synergized with ALK TKI (Figure 5a, CompuSyn combination index (CI) crizotinib+ IFNγ < 1.0 for all three). Addition of IFNγ resulted in increased pSTAT1 and expression of IRF1 and IRF7 (Figure 5b). Finally, our findings also predict that enhancement of STAT1 activation during NPM1-ALK overdose would increase toxicity. We therefore washed out drug-addicted resistant lines from ALK TKI and plated them in vehicle, IFNγ, or back in TKI (crizotinib). IFNγ significantly enhanced the death of these cells compared to the baseline death state of vehicle alone (Figure 5c). STAT1 activation therefore drives cell death during overdose signaling by NPM1-ALK in drug-addicted lymphoma cells.

Intermittent dosing prolongs control of patient-derived tumors in vivo

We previously showed resistant/addicted ALK-positive ALCL cell-line xenografts require TKI for growth in vivo and undergo cycles of growth and regression in response to discontinuous dosing,[7] but there have been no previous studies of ALK TKI in ALCL using PDX models. We therefore employed the novel ALK-positive ALCL PDX DN03 (obtained from G. Inghirami, Weill-Cornell Medical College). This PDX was established from diagnostic tumor sample (inguinal lymph node) from a 53-year-old patient with *NPM1-ALK*-positive ALCL. The patient had aggressive stage 4 disease at diagnosis, had progressive disease in response to frontline combination chemotherapy, and later died after failure of third-line treatment. We first assessed response to ALK TKI in this model by engrafting animals and dividing them to treatment with vehicle (n=11) or ceritinib 20 mg/kg oral daily (n=22). Tumors grew rapidly without treatment (vehicle median overall survival (OS) 5 days), were initially highly sensitive to ceritinib, but developed resistance (ceritinib median OS 37 days, Figure 6a). To assess NPM1-ALK and downstream signaling in resistant tumors, we made lysates from six, two of which we harvested from animals taken off TKI treatment for seven days prior to harvest. Immunoblotting showed 5/6 resistant tumors had elevated NPM1-ALK compared to control untreated tumors (Figure 6b). Note accumulation of over-expressed NPM1-ALK as a high molecular weight perinuclear aggregate band, which is well-described.[7,48] In addition, the tumors withdrawn from TKI prior to harvest demonstrate strong induction of pY701-STAT1. To assess for other resistance mechanisms in these tumors, we Sanger sequenced a 1692-bp cDNA RT-PCR product amplified from *NPM1-ALK* mRNA, including the entire kinase domain region affected by previously described TKI-resistance mutations (not shown, see methods for PCR and sequencing primers). This revealed wild-type *ALK* sequence in the original untreated tumor and all six resistant tumors shown in in 6b. *NPM1-ALK* over-expression therefore arose commonly to drive resistance in vivo in this PDX model of high-risk ALK-positive ALCL, while the effect on pSTAT1 of drug withdrawal validated our in vitro studies that TKI withdrawal from NPM1-ALK over-expressing tumors activates STAT1.

Because these two tumors showed signs of tumor regression during the week their host animals were not receiving TKI, we undertook a more comprehensive evaluation of intermittent dosing. We also wanted to test the effect of IFNγ during breaks from TKI. We engrafted resistant tumors from 6a to additional mice and divided them to continuous

ceritinib from day 1 (n=5), two-week on/off intermittent ceritinib (n=6), and intermittent ceritinib + IFNγ 3x weekly during ceritinib breaks (n=7) and followed tumor volume (TV) by ultrasound. Continuously treated animals experienced significant tumor growth beginning day 20–25 and reached predetermined TV endpoint ≥1500 mm^3 days 36–51 (Figure 6c, Supplementary Figure 5). Tumors in intermittently treated animals, by contrast, went through cycles of growth and regression as TKI cycled on and off. Overall survival was substantially increased in both intermittent groups compared to continuous (p=0.0061 cont. vs. int., p=0.0003 cont. vs int+ IFNγ, Figure 6d). There was no OS benefit, however, from use of IFNγ during TKI breaks (p=0.8749 int. vs. int.+ IFNγ). These data therefore demonstrate prolonged control of aggressive, high-risk ALK-positive ALCL through intermittent ALK TKI dosing compared to continuous and validate STAT1 activation in vivo when TKI is withdrawn from NPM1-ALK-overexpressing resistant tumors.

Discussion

Activated STAT1 is well-established as an antagonist of oncogenic STAT3, driving tumor-suppressive pro-apoptotic gene expression opposing the STAT3 survival program to which ALK-positive ALCL is addicted.[19,49,50] Interestingly, however, STAT1 activation at lower levels also helps promote ALK-positive ALCL oncogenesis, contributing to expression of the anti-apoptotic protein MCL1.[51] Wu and colleagues previously showed STAT1 is a direct phospho-substrate of NPM1-ALK, tending to drive it toward proteasomal degradation in the cytoplasm.[38] Interestingly, pSTAT3 is more favorably imported to the nucleus than pSTAT1 when both are present in the cytoplasm,[52] which might explain the delicate balance between STAT1 activation and degradation necessary for survival in ALCL's baseline state. Our data show this delicate balance is lost in NPM1-ALK-overexpressing cells withdrawn from TKI. pSTAT1 rises rapidly and dramatically, as does expression of its downstream target, the pro-apoptotic transcription factor IRF1 (Figure 4a). RNA-seq analysis shows the STAT1 expression program turns on strongly as STAT3's survival program is lost (Figure 4b). We therefore discover the reason for TKI addiction in ALCL cells over-expressing NPM1-ALK, providing the missing mechanism for this well-described phenomenon.[7,13,14] Strikingly, this is entirely distinct from the previously described mechanism of cancer drug addiction in MEK/ERK-driven solid tumors.[6,53] We emphasize that this mechanism applies only in the case of tumors that develop resistance with overexpression the NPM1-ALK drug target and not those with other resistance mechanisms that maintain baseline NPM1-ALK levels. *ALK* kinase-domain mutations were detected in some resistant tumors in one small study of ALK-positive ALCL patients treated with crizotinib,[54] but comprehensive analysis of ALK-TKI resistance has not been undertaken in this disease. Both *ALK* kinase-domain mutations and activation of bypass pathways are well-described in ALK-positive NSCLC.[10]

Most importantly, we demonstrate in vivo therapeutic implications amenable to rapid translation to clinical evaluation. Using a high-risk ALK-positive ALCL PDX model, we find intermittent dosing of ALK TKI promoted significantly improved OS in tumor-bearing animals (Figure 6d). We also found that NPM1-ALK overexpression occurred in vivo as tumors became TKI resistant and that resistant tumors withdrawn from TKI had strong activation of pSTAT1 during regression of growth (Figure 6b). Intermittent dosing is a therapeutic strategy requiring no new drug development and carrying, if anything, reduced

side effects compared to standard continuous dosing. Enhancement of STAT1 activation, and therefore the antitumor effects of TKI withdrawal, through the use of IFNγ was active in vitro (Figure 5a–c) but did not improve OS in vivo (Fig 6d). Further studies to optimize IFNγ dosing, however, which are underway in our laboratory, could validate this strategy in the future. Our IFNγ dose (20,000 units s.c.) was calculated as weight-based equivalent to starting human dosing of Actimmune ®, the clinically approved form of IFNγ, but many patients tolerate significantly higher dosing than the baseline. Regardless, clinical evaluation of therapeutic strategies defined in this report can proceed using approved drugs alone.

We do not exclude a role for additional phospho-targets that were uniquely associated with the NPM1-ALK overactivation death state in our phosphoproteomics data (Figure 3c–d). Given the overwhelming accumulation of pSTAT1 upon TKI withdrawal (Figure 4a), corresponding expression changes in both STAT1 and STAT3 target genes (Figure 4b), and rescue by STAT1 shRNA knockdown (Figure 4d), we believe additional targets likely have minor roles, if any. Reasons for the particularly high accumulation of pSTAT1 upon NPM1-ALK overactivation also are not entirely clear from these data. Possibilities include saturation of proteasomal degradation of pSTAT1 in the cytoplasm and a feed-forward accumulation of pSTAT1 since *STAT1* itself is one of its target genes. Though outside the scope of this report, these questions are highly appropriate in follow-up. Overall, our mechanistic studies re-emphasize STAT1's potent tumor-suppressive function when strongly activated. Even though high levels of oncogenic pSTAT3 also remained present, its gene-expression program was thwarted as the pSTAT1 program took over and drove cells to apoptosis. We hope novel strategies aimed at STAT1 activation to thwart STAT3, which remains a major clinically undruggable target in cancer therapeutics,[55] will receive consideration as a result of these studies.

Materials and Methods

Cell Culture

ALK-positive ALCL patient derived cell lines, Karpas-299, SU-DHL-1, SUP-M2, L-82, DEL and SR-786 were purchased from DSMZ and verified by STR fingerprinting. Culture media for Karpas-299, SU-DHL-1, DEL and L-82 was RPMI 1640 supplemented with 10% Fetal Bovine Serum (FBS), Penicillin/Streptomycin (P/S) and mycoplasma inhibitor Plasmocin prophylactic (P/P) (ant-mpp). SUP-M2 was cultured in the same media supplemented with 20% FBS,P/S,P/P. SR-786 was cultured in same media supplemented with 15% FBS,P/S,P/P. Phoenix cells were cultured in DMEM media supplemented with 10% FBS,P/S,P/P.

Cell viability

Cells were seeded at 3,000 cells per well in a 96-well plate under serial dilutions of drug. Viability was assessed at 72 hours unless otherwise mentioned using Cell Titer Glo (Promega G7573) according to manufacturer's protocol. Luminescence was measured using BioTek Synergy HT plate reader. IC50s were calculated using nonlinear fit regression analysis in GraphPad Prism8.

Protein Extraction and Western Blotting

500,000 cells/ml were seeded and incubated as mentioned. Cells were pelleted and washed once with ice-cold PBS. Proteins were extracted using RIPA (50 mmol/L Tris-HCL pH 8.0, 150 mmol/L NaCl, 1% NP40, 0.5% sodium deoxycholate, and 0.1% SDS), 7 x protease inhibitor (Thermo Scientific 1862209), Halt phosphatase inhibitor (Thermo Scientific 1862495) and Triton X-100. Proteins were extracted and quantified using BCA assay (Thermo 23208). 30 ug of proteins was loaded in each well for western blotting and developed using autoradiography films (VWR 30101) after incubation with antibodies. Primary antibodies were all used at a concentration of 1:1000 and secondary antibodies were used at a concentration of 1:10,000.

Inhibitors

The following inhibitors were used: Crizotinib (PF-02341066) (Selleckchem S106), Ceritinib (LDK378) (Selleckchem S7083), Alectinib (CH5424802) (Selleckchem S2762), Lorlatinib (PF-6463922) (Selleckchem S7536), Selumetinib (AZD6244) (Selleckchem S1008), Trametinib (GSK1120212) (Selleckchem S2673), Tofacitinib Citrate (CP-690550) (Selleckchem S5001), AZD1480 (Selleckchem S2162), Rapamycin (Selleckchem S1039), LY294002 (Selleckchem S1105), JNK-IN-8 (Selleckchem S4901), Ro-31-8220 (Selleckchem 7207), AZD5363 (Selleckchem S8017), Ipatasertib (Selleckchem S2808), SCH772984 (Selleckchem S7101), Ulixertinib (Selleckchem S7854). BKM120 and Tepp-46 were kind gifts from Dr. Thomas Craig, NCI, Bethesda, Maryland, USA; recombinant human interferon-gamma, IFNγ (BioLegend 570208).

Microscopy

Plates were first coated with Cell-Tak (Corning 354240) and allowed to dry. Cells were then seeded at 100,000 cells/ml and treated with either vehicle or drug. Cells were then live-imaged every 4 hours at 10x objective (100x magnification) in the light field using the IncuCyte Zoom (Essen Bioscience). Images were collected and analyzed using the ImageJ software.

RNA-Seq

Samples from parental and addicted lines with and without incubation in 100 nM ceritnib underwent quality control using an Agilent Bioanalyzer and Ion-Torrent Next-Gen sequencing was performed on the samples. Transcript reads were trimmed using the trimmomatic program the RedHat pipeline was used for downstream analysis. FDR cut off was at 5% and the p-value used for significance was 0.05. Statistical analysis software R (version 3.3.1) was used to plot z-scores of the analyzed data as a heatmap using the built-in package “heatmap”.

Phosphoproteomics

For comparative analysis, the parental cells were treated with drug for 12 hours and the resistant lines were withdrawn from drug for 12 hours. Protein was extracted from fresh lysates. After trypsin digestion, the proteins were processed by Metal Oxide Affinity Chromatography (MOAC) using Titanium dioxide, and the hydrophobic and hydrophilic

fractions were eluted, dried and immunoprecipitated for phospho-tyrosine. Enriched phosphoproteins were identified using mass spectrometry as previously described [27,31]. The significance threshold in the analysis was set at 5%.

PDX in vivo studies

All animal studies were performed under approval of the University of Miami Institutional Animal Care and Use Committee (IACUC). All mice used in this study were males greater than 8 weeks of age. We obtained the DN03 model under material transfer agreement from Dr. Giorgio Inghirami at Weill-Cornell Medical College. We passaged the tumor in vivo only in NOD scid gamma (NSG) mice through surgical dorsal tumor implantation, used also to initiate treatment experiments. We measured TV by ultrasound (Vevo 3100, Visualsonics), with TV ≥1500 mm3 a predetermined survival endpoint. No blinding was done for the studies carried out. Ceritinib treatment was at 20 mg/kg daily by oral gavage. This was the maximum tolerated dose (MTD) of this drug in this strain in our experience. Human IFNγ was dosed subcutaneously (s.c.) 3 times weekly at 20,000 units/dose.

Sanger sequencing was performed on cDNA amplified from mRNA extracted from treated tumors plus one of the control tumors shown in Fig. 6b to assess for TKI-resistance mutations in the *ALK* kinase domain. First, total RNA was extracted using the *Qiagen AllPrep DNA/RNA Mini Kit.* PCR amplification of the *ALK* portion of the *NPM1-ALK* fusion transcript was performed using the mRNA specific primers, ALK-forward 5’gtgtaccgccggaagcaccaggagc3’ and ALK-reverse 5’gggcccaggctggttcatgctattc3’ and the Applied Biosystems *Taqman Reverse Transcription kit*, which produced a predicted 1692-bp product for all tumors. We purified this product from agarose gels using the *Omega E.Z.N.A. Gel Extraction Kit* and submitted then for Sanger Sequencing using primers covering the *ALK* kinase domain from −12-bp to +950-bp. Primers are: ALK-1 5’cggaaaaacatcaccctcat3’, ALK-2 5’ggggagacctcaagtccttc3’ and ALK-3 5’ggtcctttggagtgctgcta3’. Results were compared to the known *ALK* mRNA sequence open-reading frame, including visual inspection of sequencing tracings when initial automated calls were uncertain (a total of four residues across the seven samples).

Area under curve

Viability data collected as previously described was run through a R-script that used the following equation for calculating the weighted area under the curve, taking into context the potency of the drug:

$$(w)pAUC = (f(AUC)/drug*peak\ concentration)/100.$$

An R script was written and run for each of the replicates run on the viability assay to obtain a weighted area under the curve and then the mean wAUC was calculated with SEM.

Synergy

Viability assays were set up as previously described. The data was then analyzed using the CompuSyn software to calculate a Combination Index (CI) which was then reported. CI <1 indicates synergy.

Statistics

Two-tailed Student's t-test was carried out for all expression data using the GraphPad Student's t- test calculator with $p < 0.05$ considered statistically significant with a 95% confidence interval, unless otherwise stated in the figure legend. All experiments reported are the mean ± SEM of three independent replicates. OS analysis employed log-rank (Mantel-Cox) statistics in Prism 8 software, with $p < 0.05$ considered significant.

Code availability

All codes were run on the open source programming environment R (version 3.3.1). The area under the curve was analyzed using the equation mentioned previously and the open-source package "AUC". The RNA-Seq was visualized as a heatmap using the open-source built-in package "heatmap".

Supplementary Material

Refer to Web version on PubMed Central for supplementary material.

Acknowledgements

This work was supported by a grant from National Institutes of Health/National Cancer Institute, 1R01CA190696-01 (J.H.S). We would also like to acknowledge the Sheila and David Fuente Graduate Program in Cancer Biology at University of Miami. S.S.R is a PhD candidate at University of Miami. This work is submitted in partial fulfillment of the requirement of the PhD. We would also like to thank Dr. Izidore Lossos, University of Miami, for his input and suggestions in writing the manuscript.

Supported by: National Institutes of Health/National Cancer Institute, 5R01CA190696-05.

References

1. Ferguson FM, Gray NS. Kinase inhibitors: the road ahead. Nature Reviews Drug Discovery 2018; 17: 353–377. [PubMed: 29545548]
2. Suda K, Tomizawa K, Osada H, Maehara Y, Yatabe Y, Sekido Y et al. Conversion from the "oncogene addiction" to "drug addiction" by intensive inhibition of the EGFR and MET in lung cancer with activating EGFR mutation. Lung Cancer 2012; 76: 292–299. [PubMed: 22133747]
3. Sun C, Wang L, Huang S, Heynen GJJE, Prahallad A, Robert C et al. Reversible and adaptive resistance to BRAF(V600E) inhibition in melanoma. Nature 2014; 508: 118–122. [PubMed: 24670642]
4. Moriceau G, Hugo W, Hong A, Shi H, Kong X, Yu CC et al. Tunable-Combinatorial Mechanisms of Acquired Resistance Limit the Efficacy of BRAF/MEK Cotargeting but Result in Melanoma Drug Addiction. Cancer Cell 2015; 27: 240–256. [PubMed: 25600339]
5. Das Thakur M, Salangsang F, Landman AS, Sellers WR, Pryer NK, Levesque MP et al. Modelling vemurafenib resistance in melanoma reveals a strategy to forestall drug resistance. Nature 2013; 494: 251–255. [PubMed: 23302800]
6. Kong X, Kuilman T, Shahrabi A, Boshuizen J, Kemper K, Song J-Y et al. Cancer drug addiction is relayed by an ERK2-dependent phenotype switch. Nature 2017; 550: 270–274. [PubMed: 28976960]
7. Amin AD, Rajan SS, Liang WS, Pongtornpipat P, Groysman MJ, Tapia EO et al. Evidence Suggesting That Discontinuous Dosing of ALK Kinase Inhibitors May Prolong Control of ALK+ Tumors. Cancer Res 2015; 75: 2916–2927. [PubMed: 26018086]
8. Morris SW, Kirstein MN, Valentine MB, Dittmer KG, Shapiro DN, Saltman DL et al. Fusion of a kinase gene, ALK, to a nucleolar protein gene, NPM, in non-Hodgkin's lymphoma. Science 1994; 263: 1281–1284. [PubMed: 8122112]

9. Kwak EL, Bang Y-J, Camidge DR, Shaw AT, Solomon B, Maki RG et al. Anaplastic Lymphoma Kinase Inhibition in Non–Small-Cell Lung Cancer. N Engl J Med 2010; 363: 1693–1703. [PubMed: 20979469]
10. Gainor JF, Dardaei L, Yoda S, Friboulet L, Leshchiner I, Katayama R et al. Molecular Mechanisms of Resistance to First- and Second-Generation ALK Inhibitors in ALK-Rearranged Lung Cancer. Cancer Discov 2016; 6: 1118–1133. [PubMed: 27432227]
11. Gambacorti-Passerini C, Messa C, Pogliani EM. Crizotinib in Anaplastic Large-Cell Lymphoma. N Engl J Med 2011; 364: 775–776. [PubMed: 21345110]
12. Mossé YP, Voss SD, Lim MS, Rolland D, Minard CG, Fox E et al. Targeting ALK With Crizotinib in Pediatric Anaplastic Large Cell Lymphoma and Inflammatory Myofibroblastic Tumor: A Children's Oncology Group Study. Journal of Clinical Oncology 2017; : JCO–2017.
13. Ceccon M, Merlo MEB, Mologni L, Poggio T, Varesio LM, Menotti M et al. Excess of NPM-ALK oncogenic signaling promotes cellular apoptosis and drug dependency. Oncogene 2015. doi:10.1038/onc.2015.456.
14. Redaelli S, Ceccon M, Zappa M, Sharma GG, Mastini C, Mauri M et al. Lorlatinib Treatment Elicits Multiple On- and Off-Target Mechanisms of Resistance in ALK-Driven Cancer. Cancer Res 2018; 78: 6866–6880. [PubMed: 30322862]
15. Adam P, Katzenberger T, Seeberger H, Gattenlöhner S, Wolf J, Steinlein C et al. A Case of a Diffuse Large B-Cell Lymphoma of Plasmablastic Type Associated With the t(2;5)(p23;q35) Chromosome Translocation. The American Journal of Surgical Pathology 2003; 27: 1473–1476. [PubMed: 14576483]
16. Onciu M, Behm FG, Downing JR, Shurtleff SA, Raimondi SC, Ma Z et al. ALK-positive plasmablastic B-cell lymphoma with expression of the NPM-ALK fusion transcript: report of 2 cases. Blood 2003; 102: 2642–2644. [PubMed: 12816858]
17. Pearson JD, Lee JKH, Bacani JTC, Lai R, Ingham RJ. NPM-ALK: The Prototypic Member of a Family of Oncogenic Fusion Tyrosine Kinases. Journal of Signal Transduction 2012; 2012: 1–14.
18. Marzec M, Kasprzycka M, Liu X, Raghunath PN, Wlodarski P, Wasik MA. Oncogenic tyrosine kinase NPM/ALK induces activation of the MEK/ERK signaling pathway independently of c-Raf. Oncogene 2006; 26: 813–821. [PubMed: 16909118]
19. Chiarle R, Simmons WJ, Cai H, Dhall G, Zamo A, Raz R et al. Stat3 is required for ALK-mediated lymphomagenesis and provides a possible therapeutic target. Nat Med 2005; 11: 623–629. [PubMed: 15895073]
20. Kodama T, Tsukaguchi T, Yoshida M, Kondoh O, Sakamoto H. Selective ALK inhibitor alectinib with potent antitumor activity in models of crizotinib resistance. Cancer Letters 2014; 351: 215–221. [PubMed: 24887559]
21. Johnson TW, Richardson PF, Bailey S, Brooun A, Burke BJ, Collins MR et al. Discovery of (10 R)-7-Amino-12-fluoro-2,10,16-trimethyl-15-oxo-10,15,16,17-tetrahydro- 2H −8,4-(metheno)pyrazolo[4,3- h][2,5,11]-benzoxadiazacyclotetradecine-3-carbonitrile (PF-06463922), a Macrocyclic Inhibitor of Anaplastic Lymphoma Kinase (ALK) and c-ros Oncogene 1 (ROS1) with Preclinical Brain Exposure and Broad-Spectrum Potency against ALK-Resistant Mutations. J Med Chem 2014; 57: 4720–4744. [PubMed: 24819116]
22. Duncan JS, Whittle MC, Nakamura K, Abell AN, Midland AA, Zawistowski JS et al. Dynamic Reprogramming of the Kinome in Response to Targeted MEK Inhibition in Triple-Negative Breast Cancer. Cell 2012; 149: 307–321. [PubMed: 22500798]
23. McDonnell SRP, Hwang SR, Rolland D, Murga-Zamalloa C, Basrur V, Conlon KP et al. Integrated phosphoproteomic and metabolomic profiling reveals NPM-ALK-mediated phosphorylation of PKM2 and metabolic reprogramming in anaplastic large cell lymphoma. Blood 2013. doi:10.1182/blood-2013-01-482026.
24. Bai R-Y, Dieter P, Peschel C, Morris SW, Duyster J. Nucleophosmin-anaplastic lymphoma kinase of large-cell anaplastic lymphoma is a constitutively active tyrosine kinase that utilizes phospholipase C-γ to mediate its mitogenicity. Molecular and cellular biology 1998; 18: 6951–6961. [PubMed: 9819383]
25. Crockett DK, Lin Z, Elenitoba-Johnson KS, Lim MS. Identification of NPM-ALK interacting proteins by tandem mass spectrometry. Oncogene 2004; 23: 2617–2629. [PubMed: 14968112]

26. Cui Y-X, Kerby A, McDuff FKE, Ye H, Turner SD. NPM-ALK inhibits the p53 tumor suppressor pathway in an MDM2 and JNK-dependent manner. Blood 2009; 113: 5217–5227. [PubMed: 19286999]
27. McDonnell SRP, Hwang SR, Basrur V, Conlon KP, Fermin D, Wey E et al. NPM-ALK signals through glycogen synthase kinase 3β to promote oncogenesis. Oncogene 2011; 31: 3733–3740. [PubMed: 22179823]
28. Houghton PJ, Kurmasheva RT, Lyalin D, Maris JM, Kolb EA, Gorlick R et al. Initial solid tumor testing (Stage 1) of AZD1480, an inhibitor of Janus kinases 1 and 2 by the pediatric preclinical testing program. Pediatr Blood Cancer 2014; : n/a–n/a.
29. Bromberg JF, Wrzeszczynska MH, Devgan G, Zhao Y, Pestell RG, Albanese C et al. Stat3 as an Oncogene. Cell 1999; 98: 295–303. [PubMed: 10458605]
30. Brunet A, Pagès G, Pouysségur J. Constitutively active mutants of MAP kinase kinase (MEK1) induce growth factor-relaxation and oncogenicity when expressed in fibroblasts. Oncogene 1994; 9: 3379–3387. [PubMed: 7936666]
31. Lim MS, Carlson ML, Crockett DK, Fillmore GC, Abbott DR, Elenitoba-Johnson OF et al. The proteomic signature of NPM/ALK reveals deregulation of multiple cellular pathways. Blood 2009; 114: 1585–1595. [PubMed: 19531656]
32. Sattu K, Hochgräfe F, Wu J, Umapathy G, Schönherr C, Ruuth K et al. Phosphoproteomic analysis of anaplastic lymphoma kinase (ALK) downstream signaling pathways identifies signal transducer and activator of transcription 3 as a functional target of activated ALK in neuroblastoma cells. FEBS Journal 2013; : n/a–n/a.
33. Xiao Y, Qiao G, Tang J, Tang R, Guo H, Warwar S et al. Protein Tyrosine Phosphatase SHP-1 Modulates T Cell Responses by Controlling Cbl-b Degradation. The Journal of Immunology 2015; 195: 4218–4227. [PubMed: 26416283]
34. Kameda H, Watanabe M, Bohgaki M, Tsukiyama T, Hatakeyama S. Inhibition of NF-κB signaling via tyrosine phosphorylation of Ymer. Biochemical and Biophysical Research Communications 2009; 378: 744–749. [PubMed: 19059208]
35. Yokoyama K, Tezuka T, Kotani M, Nakazawa T, Hoshina N, Shimoda Y et al. NYAP: a phosphoprotein family that links PI3K to WAVE1 signalling in neurons. The EMBO Journal 2011; 30: 4739–4754. [PubMed: 21946561]
36. Croucher DR, Hochgräfe F, Zhang L, Liu L, Lyons RJ, Rickwood D et al. Involvement of Lyn and the Atypical Kinase SgK269/PEAK1 in a Basal Breast Cancer Signaling Pathway. Cancer Res 2013; 73: 1969–1980. [PubMed: 23378338]
37. Rickert KW, Patel SB, Allison TJ, Byrne NJ, Darke PL, Ford RE et al. Structural Basis for Selective Small Molecule Kinase Inhibition of Activated c-Met. J Biol Chem 2011; 286: 11218–11225. [PubMed: 21247903]
38. Wu C, Molavi O, Zhang H, Gupta N, Alshareef A, Bone KM et al. STAT1 is phosphorylated and downregulated by the oncogenic tyrosine kinase NPM-ALK in ALK-positive anaplastic large-cell lymphoma. Blood 2015; 126: 336–345. [PubMed: 25921060]
39. Shuai K, Stark GR, Kerr IM, Darnell JE. A single phosphotyrosine residue of Stat91 required for gene activation by interferon-gamma. Science 1993; 261: 1744–1746. [PubMed: 7690989]
40. Shuai K, Ziemiecki A, Wilks AF, Harpur AG, Sadowski HB, Gilman MZ et al. Polypeptide signalling to the nucleus through tyrosine phosphorylation of Jak and Stat proteins. Nature 1993; 366: 580. [PubMed: 7504784]
41. Tamura T, Ishihara M, Lamphier MS, Tanaka N, Oishi I, Aizawa S et al. An IRF-1-dependent pathway of DNA damage-induced apoptosis in mitogen-activated T lymphocytes. Nature 1995; 376: 596. [PubMed: 7637809]
42. Tanaka N, Ishihara M, Kitagawa M, Harada H, Kimura T, Matsuyama T et al. Cellular commitment to oncogene-induced transformation or apoptosis is dependent on the transcription factor IRF-1. Cell 1994; 77: 829–839. [PubMed: 8004672]
43. Tanaka N, Ishihara M, Lamphier MS, Nozawa H, Matsuyama T, Mak TW et al. Cooperation of the tumour suppressors IRF-1 and p53 in response to DNA damage. Nature 1996; 382: 816. [PubMed: 8752276]

44. Gardeux V, Achour I, Li J, Maienschein-Cline M, Li H, Pesce L et al. 'N-of-1-pathways' unveils personal deregulated mechanisms from a single pair of RNA-Seq samples: towards precision medicine. J Am Med Inform Assoc 2014; 21: 1015–1025. [PubMed: 25301808]
45. Satoh J, Tabunoki H. A Comprehensive Profile of ChIP-Seq-Based STAT1 Target Genes Suggests the Complexity of STAT1-Mediated Gene Regulatory Mechanisms. Gene Regul Syst Bio 2013; 7: GRSB.S11433.
46. Carpenter RL, Lo H-W. STAT3 Target Genes Relevant to Human Cancers. Cancers 2014; 6: 897–925. [PubMed: 24743777]
47. Sironi JJ, Ouchi T. STAT1-induced Apoptosis Is Mediated by Caspases 2, 3, and 7. J Biol Chem 2004; 279: 4066–4074. [PubMed: 14623896]
48. Bonvini P, Dalla Rosa H, Vignes N, Rosolen A. Ubiquitination and proteasomal degradation of nucleophosmin-anaplastic lymphoma kinase induced by 17-allylamino-demethoxygeldanamycin: role of the co-chaperone carboxyl heat shock protein 70-interacting protein. Cancer Research 2004; 64: 3256–3264. [PubMed: 15126367]
49. Piva R, Agnelli L, Pellegrino E, Todoerti K, Grosso V, Tamagno I et al. Gene Expression Profiling Uncovers Molecular Classifiers for the Recognition of Anaplastic Large-Cell Lymphoma Within Peripheral T-Cell Neoplasms. JCO 2010; 28: 1583–1590.
50. Pensa S, Regis G, Boselli D, Novelli F, Poli V. STAT1 and STAT3 in Tumorigenesis: Two Sides of the Same Coin? Landes Bioscience, 2013 https://www.ncbi.nlm.nih.gov/books/NBK6568/ (accessed 5 Sep2018).
51. Prutsch N, Gurnhofer E, Suske T, Liang HC, Schlederer M, Roos S et al. Dependency on the TYK2/STAT1/MCL1 axis in anaplastic large cell lymphoma. Leukemia 2018; : 1.
52. Haan S, Keller JF, Behrmann I, Heinrich PC, Haan C. Multiple reasons for an inefficient STAT1 response upon IL-6-type cytokine stimulation. Cellular Signalling 2005; 17: 1542–1550. [PubMed: 15935617]
53. Hong A, Moriceau G, Sun L, Lomeli S, Piva M, Damoiseaux R et al. Exploiting Drug Addiction Mechanisms to Select against MAPKi-Resistant Melanoma. Cancer Discov 2018; 8: 74–93. [PubMed: 28923912]
54. Passerini CG, Farina F, Stasia A, Redaelli S, Ceccon M, Mologni L et al. Crizotinib in Advanced, Chemoresistant Anaplastic Lymphoma Kinase–Positive Lymphoma Patients. JNCI J Natl Cancer Inst 2014; 106: djt378–djt378. [PubMed: 24491302]
55. Beebe JD, Liu J-Y, Zhang J-T. Two decades of research in discovery of anticancer drugs targeting STAT3, how close are we? Pharmacology & Therapeutics 2018. doi:10.1016/j.pharmthera.2018.06.006.

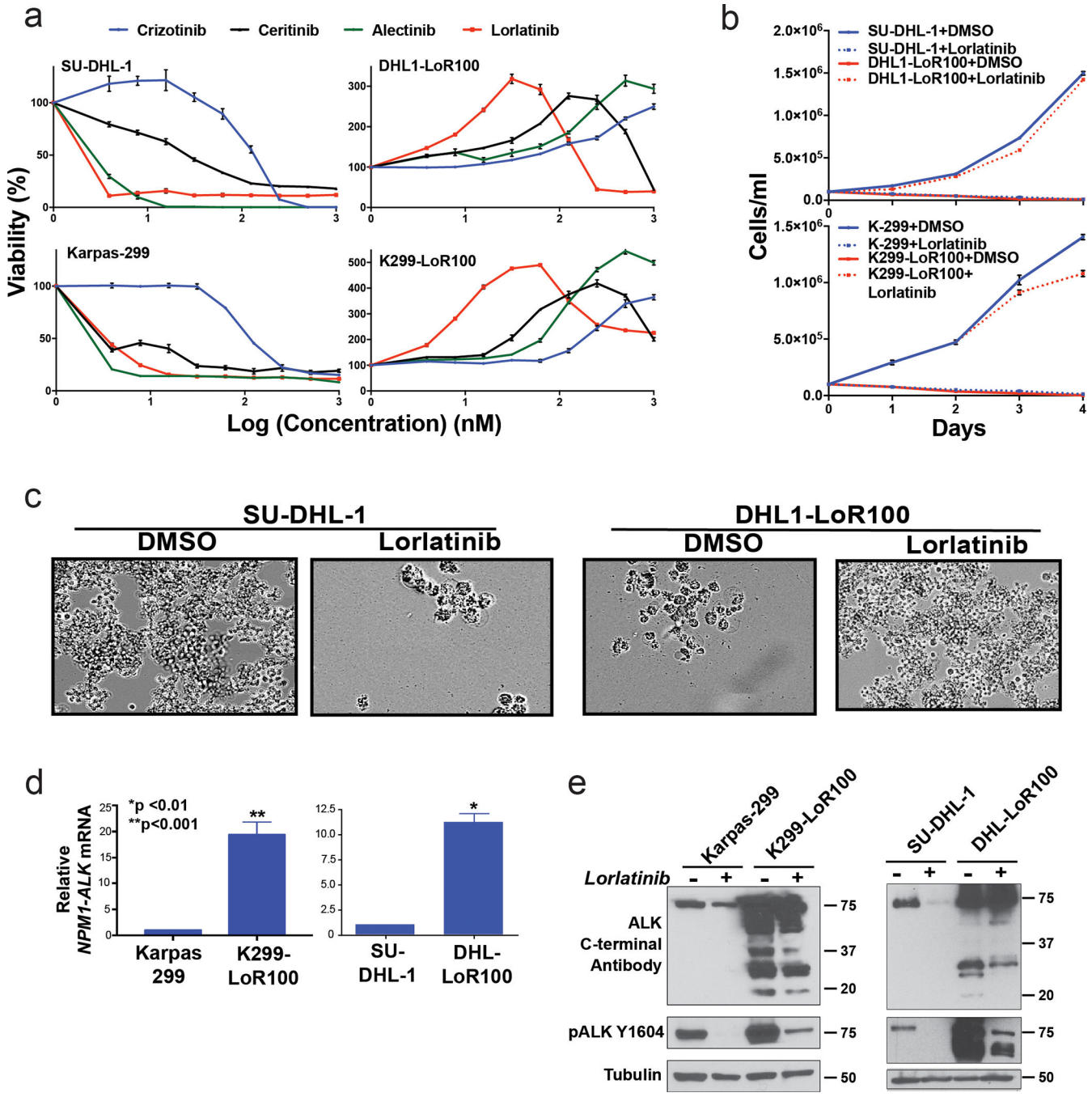

Figure 1.

Co-selection for resistance and drug addiction by lorlatinib in ALK-positive ALCL. **(a)** Viability response of parental NPM1-ALK-positive ALCL lines SU-DHL-1 and Karpas-299 (left panels) compared to lorlatinib-resistant LoR100 derivative lines (right panels) showing bell-shaped stimulation by all ALK inhibitors in the derivative lines. Cells were plated 3,000 cells per well in serial dilutions of drug, top concentration 1 μM, for 72 hours and assessed with a luminescence viability assay normalized to vehicle (DMSO)-treated. Results are technical quadruplicates ±SEM, representative of at least three independent experiments. **(b)**

Proliferation of parental and LoR100 cell lines in 1:1000 DMSO or 50 nM lorlatinib. Cells were plated at 100,000/mL and counted daily by trypan-blue exclusion. Results are mean ±SEM of three biologic replicates. **(c)** Live-cell microscopy images taken on Day 4 of parental and resistant cells treated as in (b). Micrographs from the full time-course are provided as Supplementary Figure 1c. **(d)** Relative expression of *NPM1-ALK* in parental and LoR subclones. Taqman qPCR targeting the *ALK* kinase domain sequence. **(e)** Western blot of parental and LoR lines with and without 50 nM lorlatinib showing preserved ALK activity in the resistant line during drug exposure (4th lanes) and overactivation upon withdrawal for 16 hours (3rd lanes).

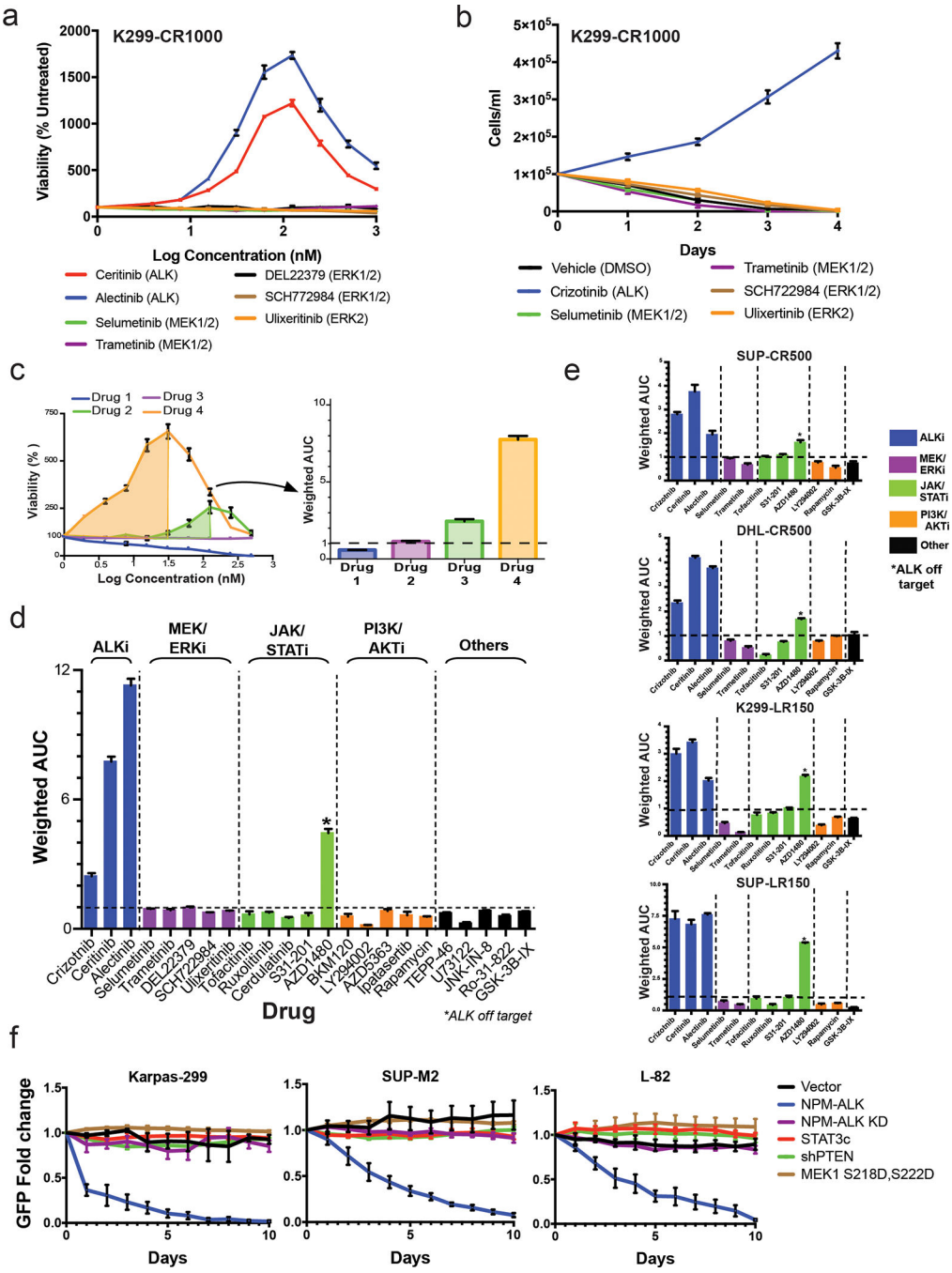

Figure 2.

ALK's canonical downstream pathways do not mediate overdose signaling. **(a)** Viability assays for drug-addicted clone K299-CR1000 washed out of ALK TKI and re-plated in serial dilutions of ALK TKIs or MEK/ERK inhibitors. Drug targets are indicated in parentheses. Viability assays were performed as in Figure 1. Shown are mean of quadruplicates ±SEM. **(b)** Proliferation assay performed as in Figure1b on K299-CR1000 cells after washout from ALK TKI followed by re-plating in vehicle or the indicated drugs. Drug concentrations (based on activity against parental cell lines) were 100 nM for

Selumetinib and Trametinib, 150 nM for SCH72294 and Ulixertinib, 500 nM for crizotinib. Only re-plating in ALK inhibitor is able to rescue proliferation compared to multiple MEK/ERK pathway inhibitors. Mean ±SEM of three independent replicate experiments. **(c)** Workflow illustrating viability curve conversion to weighted area under the curve (wAUC): Hypothetical inhibitor 2 shows no effect positive or negative at any concentration. By design, this yields wAUC=1.0 (see methods). Inhibitor 1, sensitive to drug, yields wAUC < 1.0. Inhibitors 3 and 4 stimulate viability and therefore have wAUC > 1.0. The value is weighted higher by the increased potency (lower concentration for peak effect) of inhibitor 4. **(d)** Weighted AUC results for drug-addicted K299-CR1000 cells, showing rescue only by drugs with ALK as primary or, in the case of JAK inhibitor AZD1480, secondary target. Results are mean of four replicates ±SEM. Raw viability curves are Figure 2a for MEK/ERK inhibitors and Supplementary Figure S1b for other drugs. **(e)** wAUC results for four additional ALK-positive ALCL cell line derivatives with the drug-addiction phenotype as previously described.[7] CR500: selected for growth in crizotinib to 500 nM, LR150 selected for growth in ceritinib (LDK378) to 150 nM. **(f)** Parental ALK-positive ALCL cell lines Karpas-299, L-82, and SUP-M2 were infected with constitutively active *STAT3C*, constitutively active *MEK1*-S2218D, S221D, or sh*PTEN* to individually activate oncogenic downstream pathways from ALK kinase activity. GFP co-expression was tracked compared to empty vector, *NPM1-ALK*, and *NPM1-ALK*-kinase dead (KD). Data shown as mean ± SEM of three independent replicates.

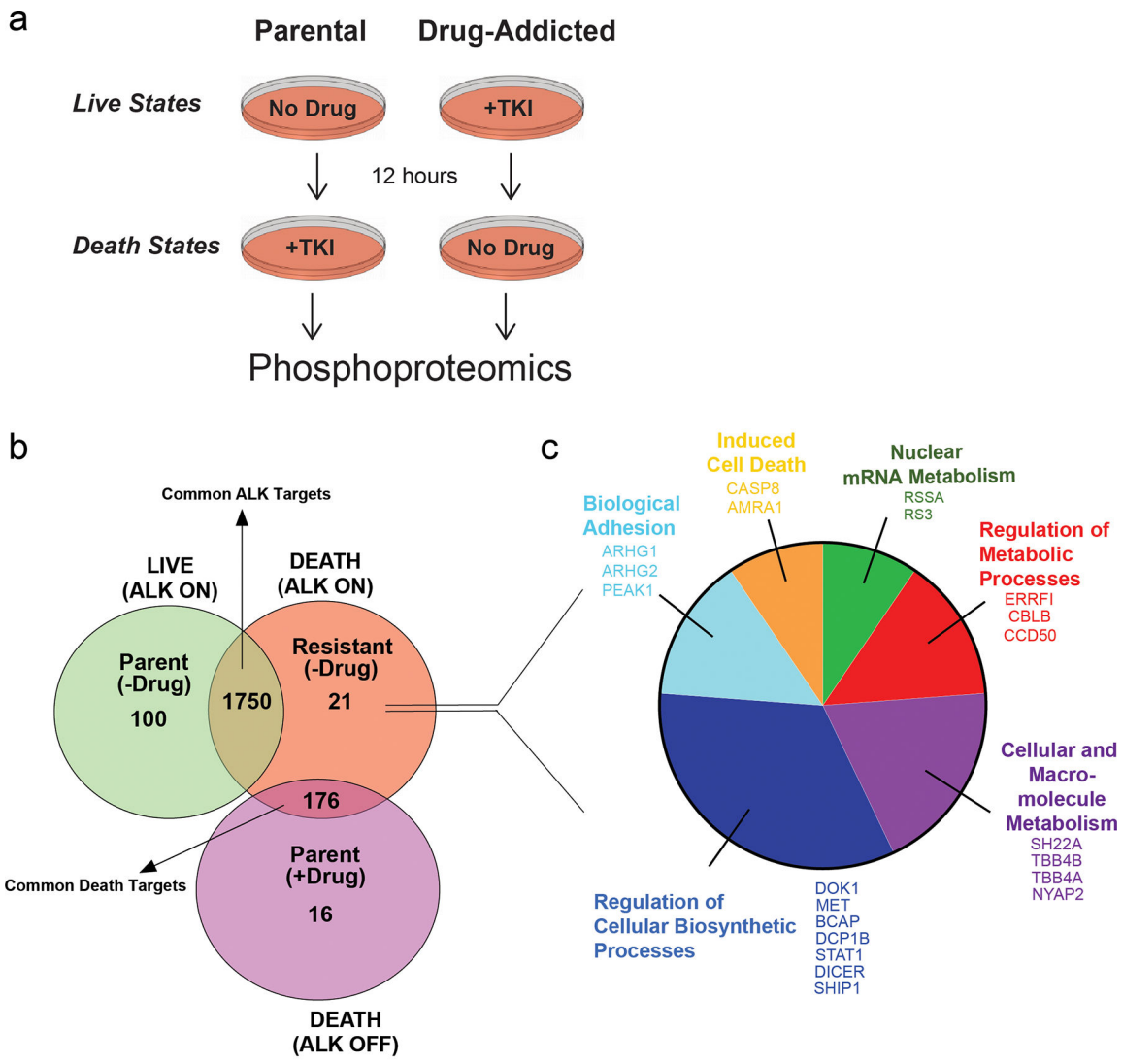

d

Gene	Protein	Phosphorylation Sites	ALK Consensus	pY Known Function
RPSA	RSSA	Y37, Y47, Y156	Y156	None
CBLB	CBLB	Y106, Y133, Y363	Y133	Autoubiquitination/degradation
CCDC50	CCD50	Y217, Y279, Y304	Y304	Inhibition
NYAP2	NYAP2	Y245, Y268	Y268	PI3K Activation in Brain
PEAK1	PEAK1	Y635, Y665	Y635	STAT3 and ERK activation
MET	MET	S966, T977, S1000, Y1003, Y1230	Y1230	Autophosphorylation site/activation
PIK3AP1	BCAP	S112, Y473	Y473	None
STAT1	STAT1	Y701, S727	Y701	Activation or degradation

Figure 3.

Phosphoproteomics yields candidate drivers of *NPM1-ALK* overdose-driven toxicity. **(a)** Overview of sample preparation for phosphoproteomics. **(b)** Upregulated phospho-proteins in K299-CR1000 cells withdrawn from TKI (ALK-on death state) were compared to the corresponding ALK-on live state (Karpas-299 untreated) and the corresponding ALK-off death state (Karpas-299 TKI treated). **(c)** This left 21 unique phospho-targets associated specifically with death induced by overactivation of NPM1-ALK. Breakdown by gene-ontology (GO) annotation as indicated. **(d)** Eight of the 21 targets had elevated

phosphorylation on a tyrosine residue in an ALK consensus phosphorylation sequence, some of which are associated with known post-translational regulatory effects. Only STAT1 Y701 is a previously described NPM1-ALK phosphorylation target. See Supplementary Figure 3 for targets without changes at ALK consensus motifs.

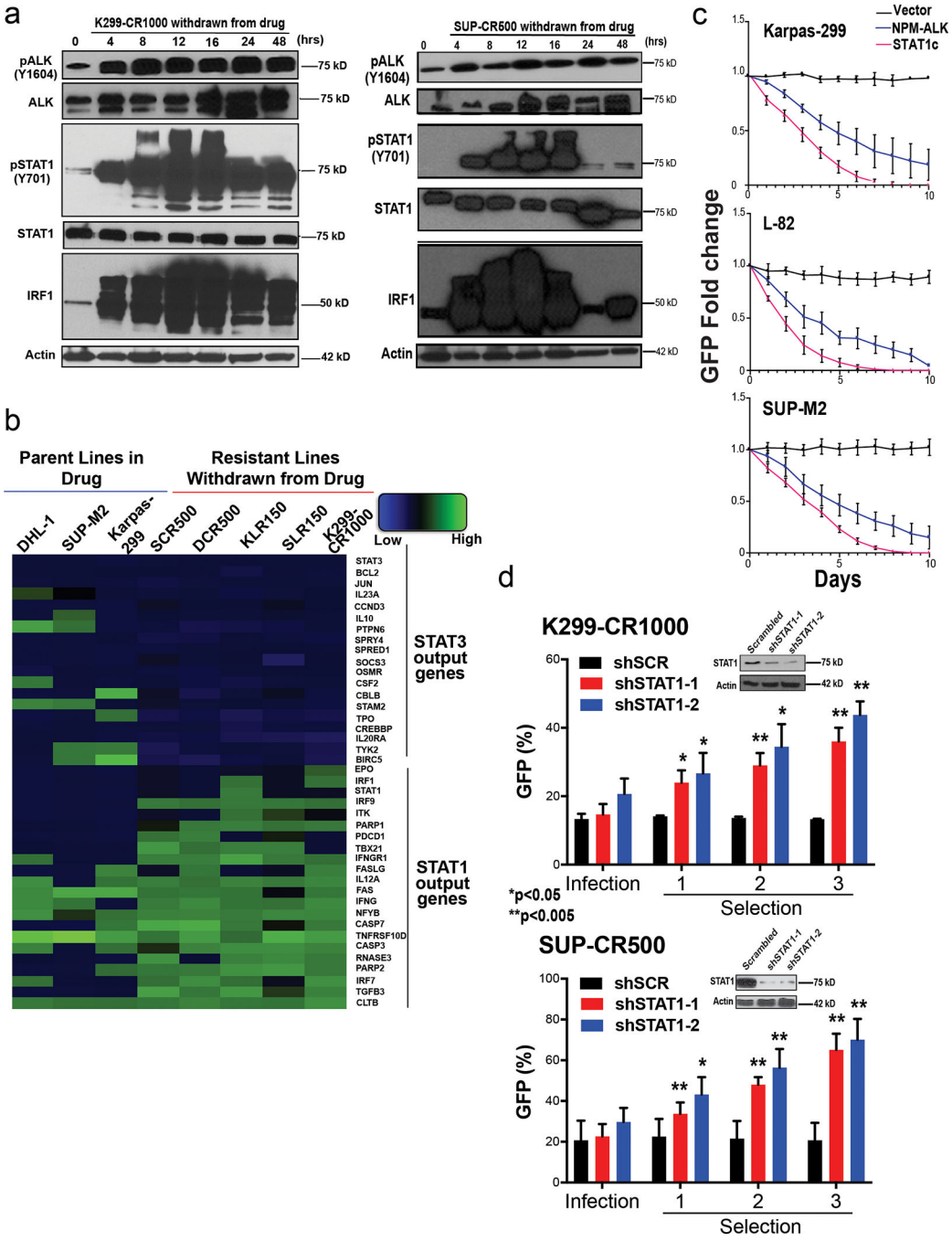

Figure 4.

STAT1 activation drives NPM1-ALK overdose-mediated cell death. **(a)** Immunoblots of TKI-addicted K299-CR1000 and SUP-CR500 maintained in TKI (time 0) or at indicated time points following washout, showing hyperactivation of STAT1 Y701 phosphorylation and induced expression of its downstream target, the pro-apoptotic transcription factor IRF1. **(b)** Gene-level RNA-Seq expression analysis for STAT1 and STAT3 target genes. Parental cells in drug vs. no-TKI parental viable state (3 left columns), resistant cells withdrawn from drug vs. TKI-maintained drug-addicted viable state (5 right columns). Supplementary Figure

4a shows the GO-annotated gene-level heat map, and gene names are in Supplementary Table 3. **(c)** Parental ALK-positive cell lines were infected with constitutively active *STAT1C* and followed via GFP co-expression compared to *NPM1-ALK* and empty vector. **(d)** We infected resistant/addicted clones K299-CR1000 and SUP-CR500 with shSCR or two different shSTAT1 sequences, took them through cycles of TKI withdrawal and rescue, and reassessed GFP co-expression after each selection. Western blotting confirmed STAT1 knockdown by both constructs in both lines (insets). Data c-d are mean ± SEM of three independent replicates. * $p<0.05$, ** $p<0.005$.

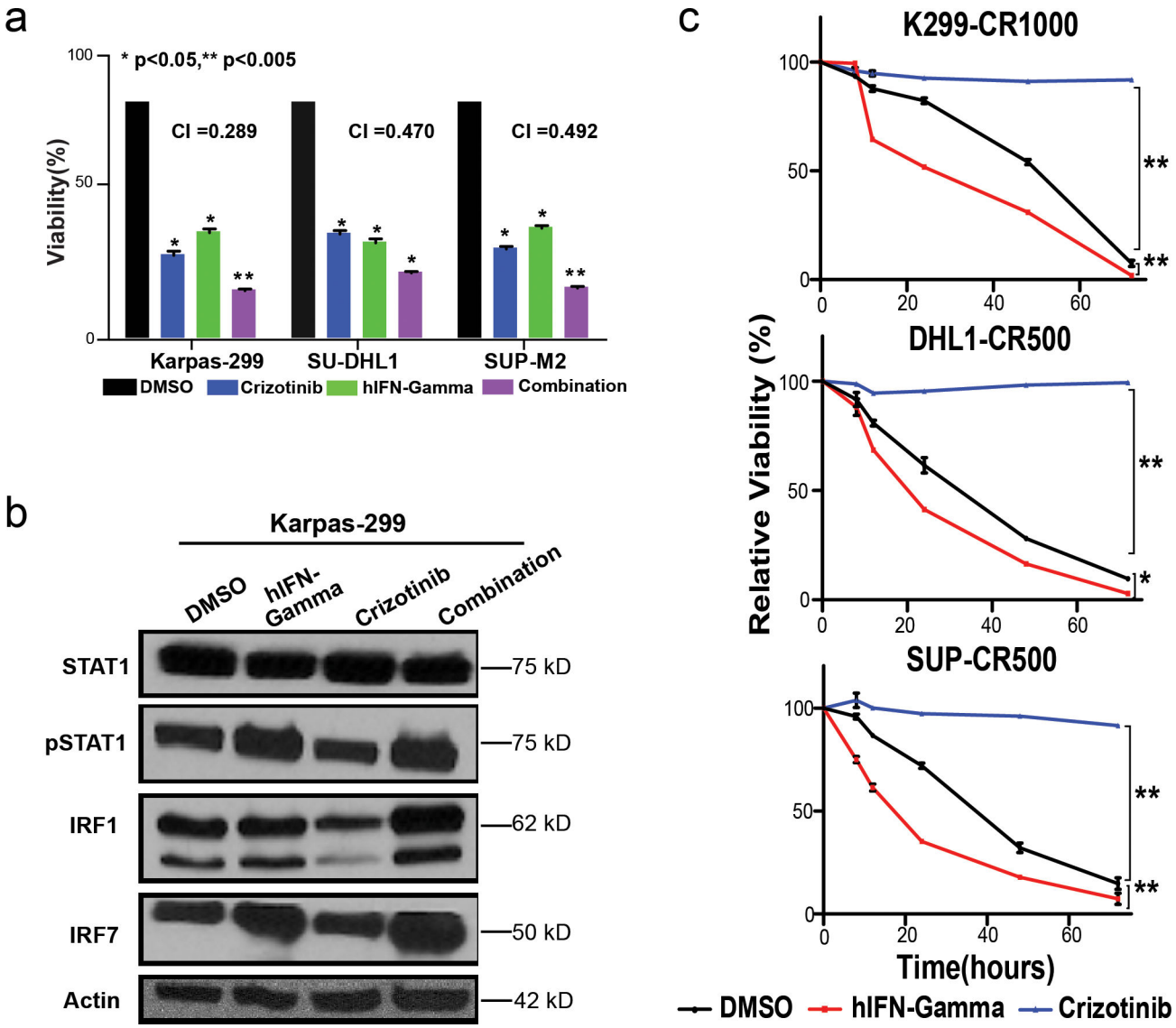

Figure 5.

Antitumor activity and STAT1 activation by IFNγ in vitro. **(a)** Parental ALK-positive cell lines were treated with vehicle (1:1000 DMSO), 50 nM crizotinib, 10 ng/ml IFNγ, or the combination with viability assessed at 72 hours. (CI: combination index assessed via CompuSyn). **(b)** Western blot showing increased pSTAT1 in response to IFNγ alone or in combination with crizotinib. **(c)** Resistant subclones K299-CR1000, SCR500, and DCR500 were withdrawn from drug and plated in vehicle (DMSO), 10 ng/ml IFNγ and 300nM crizotinib. Viability was assessed after 8, 12, 24, 48 and 72 hours.

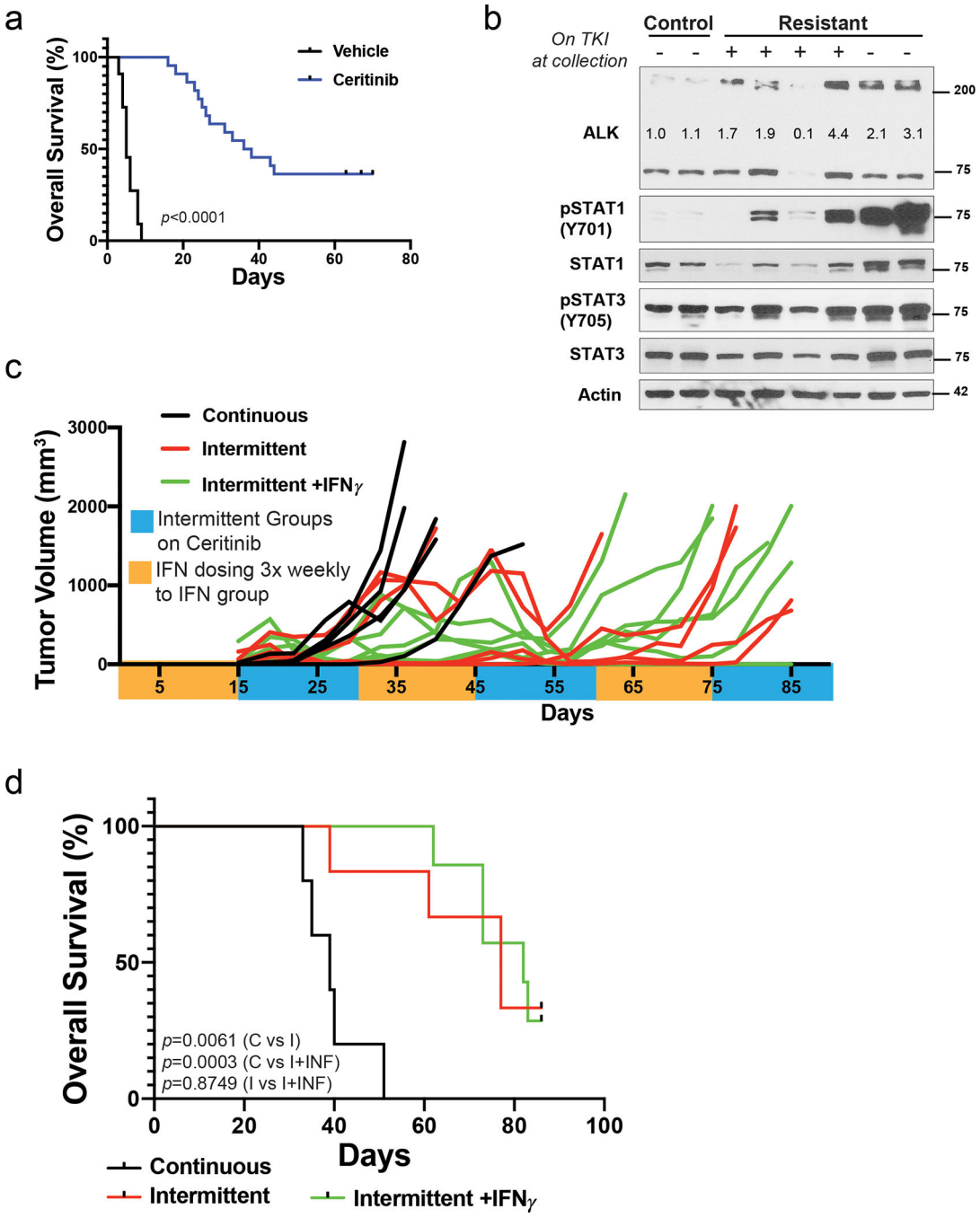

Figure 6.

TKI resistance and intermittent dosing in an ALK-positive ALCL PDX model. **(a)** We implanted NSG mice with tumors from the ALK-positive ALCL PDX model DN03, followed them without treatment (n=11) or during daily ceritinib, 20 mg/kg oral gavage (n=22), and tracked overall survival. Predetermined survival endpoints were tumor volume (TV) ≥ 1500 mm^3, weight loss > 20%, or other signs of morbidity. **(b)** We immunoblotted DN03 tumor lysates from 2 untreated animals (control) and 6 whose tumors grew through ceritinib treatment (resistant), of which 4 were on treatment at time of tumor harvest and 2

had been off treatment for 7 days (lanes 7–8) with regression of TV after drug discontinuation. Numbers indicate actin-normalized relative ALK quantification in ImageJ 2.0 software. **(c)** We harvested and engrafted TKI-resistant tumors from (a) to additional mice and divided them to continuous daily ceritinib (n=5), intermittent ceritinib 2 weeks on/off (n=6), and intermittent +IFNγ 20,000 units subcutaneously 3x weekly during ceritinib breaks (n=7) and tracked tumor volume by ultrasound. **(d)** Overall survival of animals in (c) with predetermined survival endpoints as in (a). (TV was the relevant endpoint in all cases.) Statistical survival analyses by the log-rank (Mantel-Cox) test with $p<0.05$ significant.